Shadow, an accompanying tool robot

Alejandro Torrejón[1*], Noé Zapata[1†], Pedro Núñez[1†], Lucas Bonilla[1†], Pablo Bustos[1†]

[1*]RoboLab, Universidad de Extremadura, Avda. de la Universidad sn, Cáceres, 10003, Extremadura,Spain.

*Corresponding author(s). E-mail(s): atorrejo@alumnos.unex.es;
Contributing authors: nzapatac@alumnos.unex.es; pnuntru@unex.es; lubonilla@alumnos.unex.es; pbustos@unex.es;
†These authors contributed equally to this work.

Abstract

This paper details the procedure of planning and constructing a new mobile, social robot, taking into account specific functional constraints. Shadow is an innovative blend of a versatile tool and a human associate. The objective is to provide companionship to its human owner during extensive work tasks in diverse settings. The design mandates a cost-effective build that is not just highly agile, but also entirely constructed via 3D printing technology. The requirement is for the robot to possess omnidirectional kinematics, complemented by a versatile power electronics system, capable of adapting to varying energy needs. Energy storage hinges on the use of lithium batteries, engineered to ensure a minimum of seven hours of autonomous functioning. An array of sensors will be integrated into the robot to constantly scrutinize the power system's status, monitor tilt and acceleration, and underpin a self-diagnostic system that evaluates this data. The adopted methodology fosters a swift generation of prototypes, which are iteratively tested, refined, and improved, aligning with the defined objectives. Throughout this procedure, several interesting issues have been identified and subsequently resolved. Shadow has transitioned from TRL2 to TRL7 in less than a year and is now been tested with different high-level functionalities.

Keywords: Mobile social robot, Cost-effective, 3D printing technology, Omnidirectional kinematics, Prototype generation

1 Introduction

Social robots are devices that must evolve rapidly to keep pace with new technological advancements and to meet users, preferences and requirements. Several factors may limit the adaptability of a given design, thereby restricting its effective lifespan. One of the most common limitations is scalability, through the addition or replacement of sensors, actuators, and computing resources. With the current influx of 3D sensors, such as 360º cameras and 3D Lidars, and the demand for more powerful embedded GPUs capable of processing large DNN models in real-time, a commercial robot with closed or restricted update options will quickly become obsolete. Another factor contributing to the obsolescence of commercial robots is human acceptability or the increasing demand for lighter, more agile designs that are quickly associated with biological movement. The recent availability of high-powered wheel-motor units and custom-configured lithium batteries has paved the way for more compact, lightweight, and efficient mobile bases. Lastly, as general-purpose social robots are still beyond the reach of current technology, the concept of 3D printing specialized body designs for specific purposes is becoming increasingly viable. Robots created with functional constraints in mind can be more effective in their designated domain of activity, more cost-effective, and more likely to evolve through successive designs into highly optimized solutions.

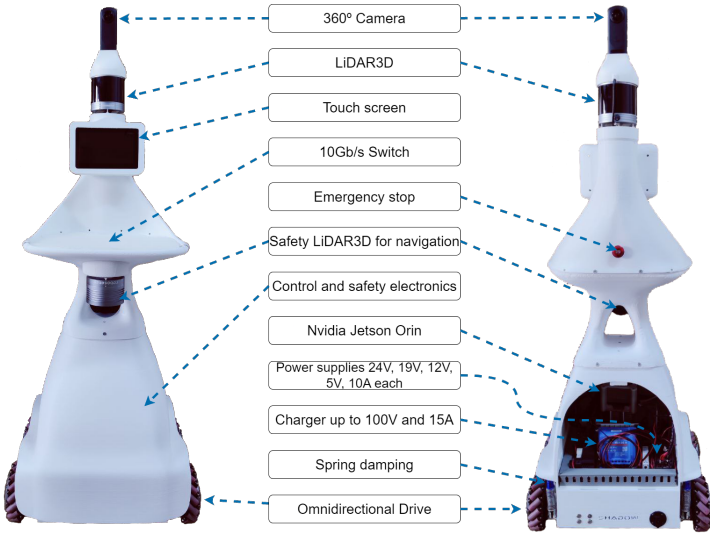

Fig. 1: Shadow elements.

The construction of the Shadow robot [1], Figure 1, is a partial response to these three types of problems. We have relayed on a quick prototyping cycle, now possible

[1]This work has been supported by a Proof of Concept project (PDC2022-133597-C41) funded by the Spanish Research Agency and is the evolution of several previous prototypes developed in former projects.

thanks to the availability of large format 3D printers, and a modular design of the power electronics.

The role of Shadow as a social robot is to serve as a smart, flexible tool for human activities such as delivery in health care or in workshop maintenance. This problem has a long history of research where questions related to the functionality and acceptance in different scenarios have been investigated in trying to find guidelines for the best possible designs [1][2][3][4]. In general, a good design entails a series of functional requirements of having a space for humans to place things, reduced size to fit in small places, high mobility to keep the pace of the person, a clean aspect without visible electronics or cables, an efficient HRI capability to interact and receive orders, a long autonomy of several hours, a set of integrated sensors that guarantee safety for itself and for people, an efficient and robust human detection, recognition and tracking capability, and, most desirably, a control architecture for visual semantic navigation, so it can reach places and objects using a human shared vocabulary. Also, as a construction and budget requirement, the robot's body had to be completely 3D-printable.

To achieve these requirements, we have iterated over a series of prototypes. This process has allowed us to detect non-evident wrong design decisions that lead to undesirable situations. These issues only became apparent once the prototype was built and tested. Two sources of error that we identified were the configuration of the volume inside the plastic casing, and the vibrations transmitted to the tray. The result of the first year of work on this robot is shown in Figure 2 as a series of prototypes. The rest of the paper goes first through a review of existing commercial and custom-made robots and then presents the development of the different parts and elements of the robot. To conclude, we describe some initial experiments in the person tracking task and energy consumption.

Fig. 2: Evolution of the robot Shadow.

2 Related Robots

As part of the design process followed with Shadow, we have analysed and compared several well-known commercial robots available for purchase, as well as some custom-made robots built at research labs. The comparison takes into account only the functionalities offered by those units and advertised by the manufacturers.

Feat/Robots	Shadow	Morphia[5]	TIAGo[6]	WaPOCHI[7]	Dinerbot T5[8]	Bellabot[9]	Amy Waitress[10]	Hobbit[11][12]	Giraff
Omnidirectional movement	✓	×	∼	×	×	×	×	×	×
Autonomous Navigation	✓	✓	✓	✓	✓	✓	✓	✓	✓
Detection of people	✓	✓	✓	✓	×	×	×	✓	✓
Object Manipulation	×	✓	∼	✓	×	×	×	✓	×
Video Calling	×	✓	✓	×	×	×	×	✓	✓
Transportation	✓	✓	✓	✓	✓	✓	✓	✓	✓
Tracking	✓	✓	✓	✓	×	×	×	✓	✓
Expansible	✓	×	∼	×	×	×	×	×	∼
Low-cost focus	✓	✓	×	×	×	✓	✓	✓	✓

Table 1: Robot comparison table
✓Available, ∼Depends on model or conditions, ×Not available

For a more extensive but similar comparison, see [13]. The table shows a great coincidence in many of the compared functionalities, however, the day-to-day use of robots in research labs implies more subtle aspects that will condition their long-term availability, such as adding of new or more powerful computers, connectivity, software updates, part replacement, adaptation to new sensors, guarantee, etc.

3 Body Design

The body of Shadow has been conceived as one large printable piece that is both the supporting structure and the functional shape for external (HRI) and internal (electronics and cables guiding) requirements. The size limitation of our 3D printer (500x500x600mm) has forced us to divide the body into three pieces and a small connecting element.

3.1 Mobile Base

To achieve high mobility, Shadow has been designed with omnidirectional kinematics using four Mecanum wheels in a rectangular configuration.

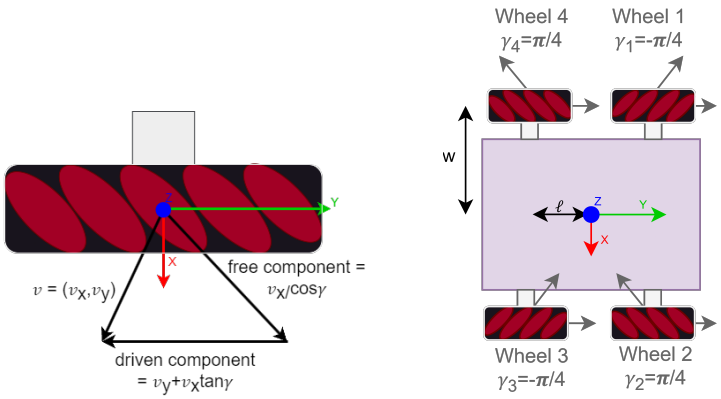

(a) Mecanum wheel.

(b) Coordinate systems in the omnidirectional base.

Fig. 3: Omnidirectional kinematics.

The inverse kinematics equations need to control the robot have been derived following [14][15]. Figure 3b shows the wheels' positions, the 45º orientation of their rollers and the robot's coordinate system.

The inverse kinematics equation of the robot can be obtained from the wheel kinematics shown in Figure 3a. At the centre of the wheel, the linear velocity $v = (v_x, v_y)$ is the sum of the velocity along the driving direction and the velocity along the sliding direction:

$$\begin{bmatrix} v_x \\ v_y \end{bmatrix} = v_{drive} \begin{bmatrix} 0 \\ 1 \end{bmatrix} + v_{slide} \begin{bmatrix} cos\gamma \\ sin\gamma \end{bmatrix} \tag{1}$$

where γ denotes the angle at which free sliding occurs allowed by the passive rollers on the circumference of the wheel, v_{drive} is the driving speed and v_{slide} is the sliding speed. Solving Equation 1 for v_{drive} and v_{slide} we get:

$$\begin{aligned} v_{drive} &= v_y\text{-}v_x \tan\gamma \\ v_{slide} &= v_x / \cos\gamma \end{aligned} \tag{2}$$

When the robot is moving with velocity $v = \begin{bmatrix} \omega_z & v_x & v_y \end{bmatrix}^\top$, each wheel u_i will have an angular speed given by:

$$u_i = \begin{bmatrix} \frac{1}{r_i} & \frac{tan\gamma_i}{r_i} \end{bmatrix} \begin{bmatrix} x_i & 0 & 1 \\ y_i & 1 & 0 \end{bmatrix} \begin{bmatrix} \omega_z \\ v_x \\ v_y \end{bmatrix} \tag{3}$$

where x_i, y_i are the coordinates of wheel u_i w.r.t. the centre of the robot, the γ_i are the angles of each roller and the r_i are the radius of each wheel. From right to left, the

first transformation expresses the linear velocity at the wheel in the robot's centre b. The second transformation calculates the driving angular velocity using Equation 2.

To obtain the final inverse kinematics equation, the position coordinates of each wheel and the angle of its roller, ± 45, are substituted in Equation 3. As an example, for wheel u_1 with $\gamma = \frac{-\pi}{4}$:

$$u_1 = \begin{bmatrix} \frac{1}{r_i} & \frac{-1}{r_i} \end{bmatrix} \begin{bmatrix} \text{-}w & 0 & 1 \\ l & 1 & 0 \end{bmatrix} = \begin{bmatrix} \text{-}w\text{-}l & \text{-}1 & 1 \end{bmatrix} \frac{1}{r_1} \tag{4}$$

Each u_i vector is stacked as rows in a matrix, to obtain Equation 5. This equation links the desired velocity of the robot's centre, v_x, v_y, ω_z, to the linear speed of the wheels, u_i. The geometric parameters w and l denote the semi-distance between wheels and the semi-distance between axes, respectively.

$$\begin{bmatrix} u_1 \\ u_2 \\ u_3 \\ u_4 \end{bmatrix} = \frac{1}{r} \begin{bmatrix} \text{-}w\text{-}l & \text{-}1 & 1 \\ w + l & 1 & 1 \\ w + l & \text{-}1 & 1 \\ \text{-}l\text{-}w & 1 & 1 \end{bmatrix} \begin{bmatrix} \omega_z \\ v_x \\ v_y \end{bmatrix} \tag{5}$$

By setting v_z and v_y to zero, the equation sends all wheels' speeds to the same value, making the robot move forward. For lateral speed, $v_y \neq 0$, wheels in the same diagonal receive the same sign in the speed magnitude. For rotation, wheels on the same side receive the same sign and a magnitude scaled by the geometric parameters.

This omnidirectional configuration has been translated to the real robot using four Mecanum motor-wheels. Each wheel includes a 200W hub motor that is controlled by one of the two 2-axis drivers provided by the same manufacturer. In the first prototype, the wheels were directly attached to the chassis. To avoid premature wear of the plastic part of the chassis holding the wheel's axis, we introduced an intermediate element made of a more resistant material, see Figure 4a. Several available plastics for the 3D printer were tested for extended periods of time working with the robot. Among the tested materials, PLA (*Polylactic acid*), ABS (*Acrylonitrile butadiene styrene*), TPU (*Thermoplastic Polyurethane*), Polycarbonate and Flex A98, and a final selection was made for TPU. This one is difficult to print, but it did not show any signs of wear or backslash after days of intensive testing, see Figure 4b.

(a) Kite tail shaped element inserted in the robot's chassis.

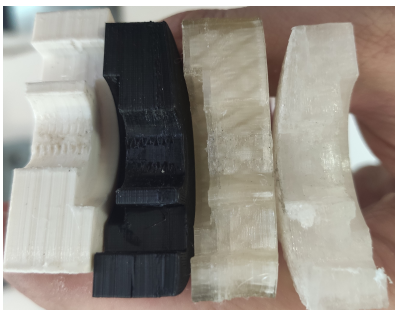

(b) State of wear of the materials after the test. From left to right, PLA, ABS, TPU and Polycarbonate.

Fig. 4: Wheel fixation solution and materials.

3.2 Suspension

The most serious problem that we encountered after the first prototype was fully assembled and tested in real conditions, was the intensity of the vibrations that were transmitted up to the tray and to the head where the camera is placed. The high-frequency movements made unusable the tray as a transportation surface for elements such as medicines, bottles, or any large vertical element. Three main causes were identified, the misalignment of the Mecanum wheels, the instability of the four-wheel configuration in which one of them usually loses contact with the floor, and the rigid connection of the motor wheels to the plastic (PLA) body. The three issues were solved by decoupling the wheels from the chassis through a micro-adjustable suspension system.

(a) Wheel without damping system.

(b) Wheel with damping system.

Fig. 5: Before and after view of the wheel suspension system.

Figure 5a shows the initial design with the wheel directly attached to the chassis.

Speed/Movement	1	2	3	4	5	6	7	8	9	10	11
Linear(axis y) Speed(mm/s)	300	0	0	0	-800	0	0	0	300	-800	0
Side(axis x) Speed(mm/s)	0	0	300	0	0	0	-800	0	300	-800	0
Rotational Speed(rad/s)	0	1	0	1	0	1	0	0.5	0	0	0.5
Execution Time(s)	10	6.25	10	1.25	3.75	6.25	3.75	0.25	5	3.75	1.25

Table 2: Sequence of movement in the vibration .

A three-axis accelerometer was placed on the chassis with a sampling rate of 4 ms and the robot was driven through several forward, lateral, diagonal and rotational movements at speeds of 800mm/s and 300mm/s. In more detail, Table 2 shows the sequence of movements and their speeds and Figure 6a shows the results. The three series represent axis x, y, z, with time running in the abscissa and displacement in millimetres per second[2] in the ordinate. High vibration values are observed in all three axes and most prominently in the z, which runs along the up-down direction of the robot, axis at a forward robot speed of 800 mm/s. After these results, a new design was undertaken to include a suspension system where each wheel is attached to a supporting plastic element, made of TPU, that moves vertically along two steel rods. The movement is constrained by two shock absorbers that link it to the chassis. The steel rods are fixated to the chassis using metal elements that can be adjusted in position effectively modifying the orientation of the wheels concerning the chassis. The shock absorbers were filled with 650 viscosity paraffin oil. The final design is shown in Figure 5b. A new series of tests were run to check that the level of vibrations was reduced. The results are shown in Figure 6c.

The tests performed with this suspension system showed a drastic reduction in the vibrations in the robot's base and transmitted to the tray. The reduction in standard deviation obtained with respect to chassis mounting was as shown in Table 3.

System/Axis	X	Y	Z
Damping system with 0,01DaN/mm springs	64.31%	10.94%	118.02%
Damping system with 0,1288DaN/mm springs	90.1%	129.87%	333.31%

Table 3: Improvement of the standard deviation with respect to chassis mounting.

With this data, a Fast Fourier Transform was computed with a time window of 1 second and a time step of 0.5 seconds[2]. The results also confirm the drastic reduction in vibrations in all relevant modes.

[2]FFT video with 1 second time window and 0.5 second time step https://youtu.be/t_bysqOqY2o

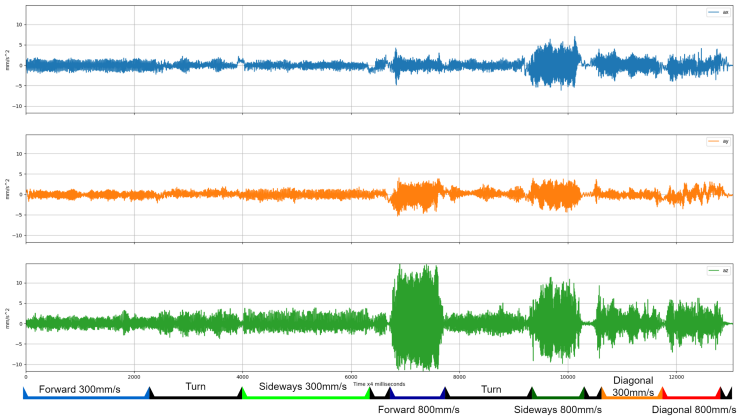

(a) Acceleration without damping system.

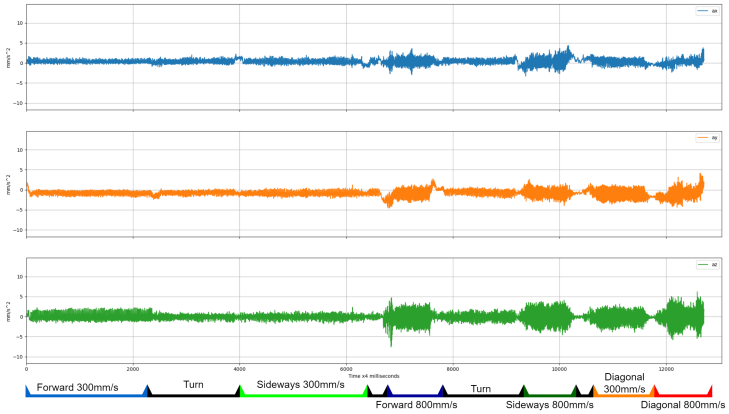

(b) Acceleration of damping system with 0.01DaN/mm springs.

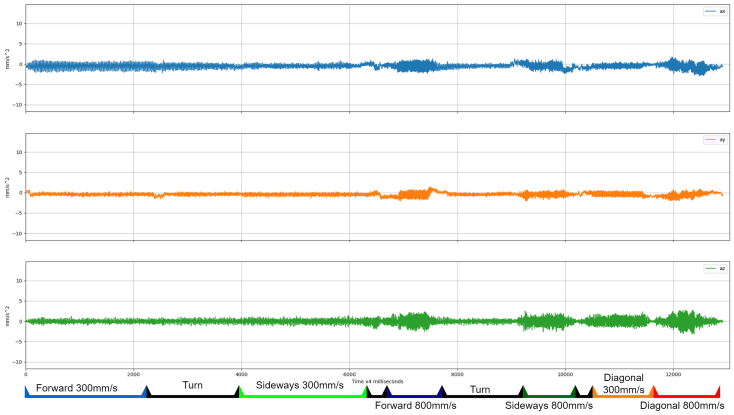

(c) Acceleration of damping system with 0.1288DaN/mm springs.

Fig. 6: Acceleration comparison.

4 Power Electronics

The power electronics that drive Shadow have been designed to avoid the usual limitations of commercial robots that come with closed or poorly documented electronics. To extend the operational life of a robot as much as possible, it should allow for the addition of new sensors and computing resources. These elements will draw energy at different voltages that have to be supplied from the robot's batteries and that may not be available in the initial design. To avoid this problem we have designed an extractable power electronics tray that provides several buses and which can be easily redimensioned, if needed, by replacing the power supplies. Table 4 shows the range of provided voltages and amperages.

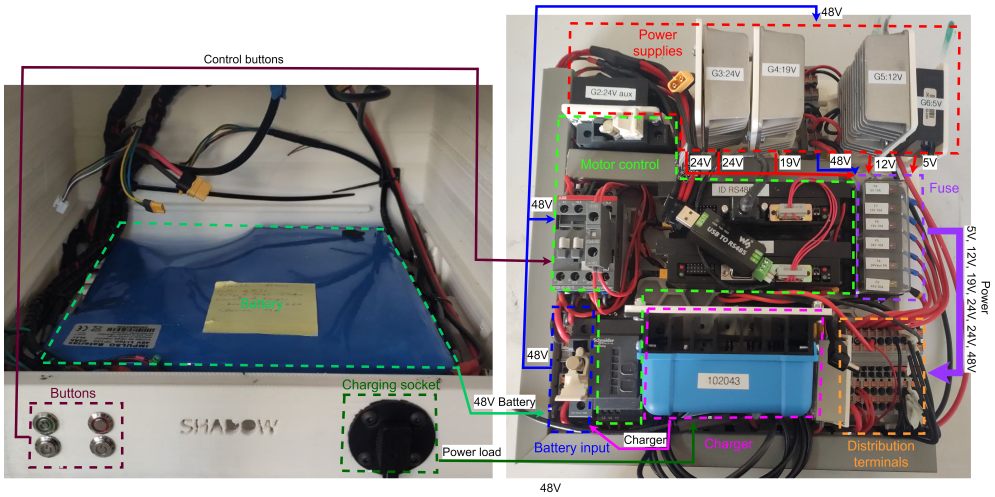

Fig. 7: Lithium battery and power schematics.

	Battery	Motors	Control	Supply	Supply	Supply	Supply	Supply
Voltage	48V	48V	24V	48V	24V	19V	12V	5V
Max. current	22A	13A	5A	20A	10A	10A	10A	10A

Table 4: Power busses.

Figure 7 shows the 1 KW/h lithium battery occupying the lowest position in the chassis, and a top view of the power tray with the different elements and their connections superimposed in varying colours. Currently, this configuration is powering the four 200W wheel motors, a Nvidia Orin unit, two 3D Lidars and a 360 RGB camera, along with other smaller sensors and devices.

5 Sensors

All sensors in the Shadow are implemented in Robocomp[16] and their distribution is divided into two sets, internal and external.

Internal sensors measure the internal state of the robot and include a voltmeter and an ammeter in each power bus, battery status and charge monitoring, the temperature in several points of the tray and an AHRS-IMU. These sensors are read by a dedicated embedded processor that creates and publishes a data structure with the robot's current internal state.

Fig. 8: 360^{o} image with LiDAR depth on jet colourmap.

External sensors give Shadow access to the outside world. The installed sensors include two 3D LiDARs and a 360^{o} camera. The LiDAR placed on the head has a more usual configuration of 32 elements covering an angle that goes from 10^{o} (upwards) to -55^{o}. The second LiDAR is a dome-type model that covers $90x360$ solid degrees. This configuration provides almost complete coverage of the volume surrounding the robot. The 360^{o} RGB camera provides a 4K H264 compressed stream and is constructed with two 180^{o} fish-eye cameras placed back to back. Figure 8 shows the output of the camera read by a dedicated robot's component.

As one of the main goals of this robot is to perform visual semantic navigation, including the tracking of its human master, it is crucial that both LiDARs are registered with the 360^{o} RGB image, so all detected visual elements can be positioned in 3D space. Given the heavy post-processing that the manufacturer of the camera includes in the final stream to provide an excellent-quality image, and the front-back configuration of the two fish-eye cameras, several steps are needed to project an arbitrary LiDAR 3D point on the 360^{o} image.

The 360^{o} camera is treated as two fisheye 180^{o} cameras placed back to back, whose images are combined into an equirectangular frame of reference. We first define a 3D coordinate system centred at each camera, $\mathfrak{C}_f$ and $\mathfrak{C}_b$.

A 3D point obtained by the LiDAR is transformed into the corresponding camera coordinate system and projected on the fisheye image plane:

Since all 2D pixels in the fisheye camera have 3D coordinates:

In these frames, an image pixel (x, y), normalized between the values [-1 ,1] in each of its 2D coordinates, has the following 3D coordinates:

$$p_x = x, \quad p_y = \frac{r}{\tan(\frac{r*a}{2})}, \quad p_z = y \tag{6}$$

where $r = \|(x, y)\|$ and a is the field of view. We can now compute a new transformation of the projected points to obtain coordinates in a longitude/latitude system as:

$$la = \arctan(\frac{p_z}{\|(p_x, p_y)\|}), \quad lo = \arctan(p_y, p_x) \tag{7}$$

And finally, the equirectangular coordinates are obtained as:

$$e_x = \frac{lo}{\pi}, \quad e_y = \frac{la * 2}{\pi} \tag{8}$$

These equirectangular coordinates are normalized and must be scaled to the image size of the 360º camera.

This algorithm can project any LiDAR 3D point on the 360º image, once the relative pose is known and both fisheye cameras are calibrated. By combining the projected points with object detectors or semantic segmentations, it is possible to assign to those visual elements an approximate position in 3D space. However, the size of the point cloud and of the 360º image makes an *all objects, all the time* policy not advisable for real-time operation. Instead, we have introduced an attentional mechanism that works similarly as an orientable camera, but with 360º coverage and no mechanical delay. This mechanism is based on a server component for each LiDAR and for the 360º camera. These components read at maximum frequency the data streams from the devices and offer an RPC interface with parameters defining the desired vertical slice of the 3D points cloud, or an arbitrary region of the global image at some specified resolution. Figure 9a shows how these selections work.

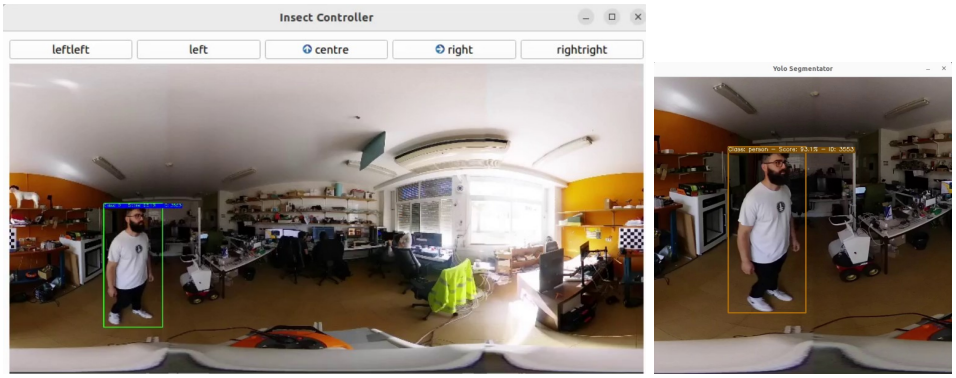

(a) Global 360° image stream.

(b) Target selected with ROI output.

Fig. 9: 360° camera component image stream outputs.

Two types of tracking can be simultaneously used. Foveal tracking is available by initially requesting a global, low-resolution region of the image is requested by the detectors. Once a target is selected, the ROI will be progressively adapted to the region of the target and tracked from there on. The position and size of the requested ROI is maintained by a PID controller. Peripheral attention to non-target, unexpected objects can be performed by requesting a large-size, low-resolution region from the server and processing it with the detectors. Both modes and the additional degrees of freedom provided by the attentional system have to be integrated in the tracking architecture.

6 Conclusion

The Shadow robot is now being tested extensively in our laboratory with results according to plan. The response to mechanical stress, vibrations and impacts is better than expected. The mobility of the platform, as human subjective perception, exceeds most of the known robots that we have built before or known through direct or recorded interactions. The autonomy can easily surpass ten hours in a mixed-use, consuming an average of 160W when moving and 70W when stationary, which opens new experimental opportunities for future developments.

We can conclude that the requirements and goals have been achieved, moving an initial design from TRL2 to TRL7 in less than one year. The path opened with Shadow shows that the 3D printing of body envelopes under functional constraints is now a valuable option for research laboratories and startups that want to build prototypes with specific custom-oriented features.The production of a Shadow robot will cost approximately 13,000 euros, 59% of which will be the LiDARs and the 360º camera, with a final weight of 32 kg.

Using this methodology, we expect to build a new robot that integrates a 7 DOF arm and has functional requirements oriented towards human-robot collaboration in healthcare environments.

Acknowledgments. This work has been partially funded by TED2021-131739-C22, supported by Spanish MCIN/AEI/10.13039/501100011033 and the European Union's NextGenerationEU/PRTR, by the Spanish Ministry of Science and Innovation PDC2022-133597-C41 and by FEDER Project 0124 EUROAGE MAS 4 E (2021-2027 POCTEP Program)

References

[1] Mast, M., Burmester, M., Kruger, K., Fatikow, S., Arbeiter, G., Graf, B., Kronreif, G., Pigini, L., Facal, D., Qiu, R.: User-Centered Design of a Dynamic-Autonomy Remote Interaction Concept for Manipulation-Capable Robots to Assist Elderly People in the Home. Journal of Human-Robot Interaction, 96–118 (2012) https://doi.org/10.5898/jhri.1.1.mast

[2] Prescott, T.J., Robillard, J.M., Ethology, C.: Designing Socially Assistive Robots : A Relational Approach Designing Socially Assistive Robots : A Relational Approach (July) (2022)

[3] Dautenhahn, K.: Socially intelligent robots: Dimensions of human-robot interaction. In: Philosophical Transactions of the Royal Society B: Biological Sciences, vol. 362, pp. 679–704. Royal Society, ??? (2007). https://doi.org/10.1098/rstb.2006.2004

[4] González-González, C.S., Violant-Holz, V., Gil-Iranzo, R.M.: Social robots in hospitals: A systematic review. Applied Sciences (Switzerland) **11**(13), 1–23 (2021) https://doi.org/10.3390/app11135976

[5] Wengefeld, T., Schuetz, B., Girdziunaite, G., Scheidig, A., Gross, H.-M.: The morphia project: First results of a long-term user study in an elderly care scenario from robotic point of view. In: ISR Europe 2022; 54th International Symposium on Robotics, pp. 1–8 (2022). VDE

[6] PALROBOTICS: TIAGO. https://pal-robotics.com/es/robots/tiago/ Accessed 2023-09-21

[7] Honda: WaPOCHI. https://global.honda/jp/stories/046/ Accessed 2023-09-21

[8] KEENON: DinerbotT5. https://www.keenonrobot.com/EN/index/Page/index/catid/6.html Accessed 2023-09-21

[9] PUDU: Bellabot. https://www.pudurobotics.com/es/products/bellabot Accessed 2023-09-21

[10] experthubrobotics: AmyWaitress. https://experthubrobotics.com/premium-robots/csj/amy-waitress Accessed 2023-09-21

[11] Fischinger, D., Einramhof, P., Wohlkinger, W., Papoutsakis, K., Mayer, P., Panek, P., Koertner, T., Hofman, S., Argyros, A., Vincze, M., Weiss, A., Gisinger, C.: Hobbit - the mutual care robot. (2013)

[12] Bajones, M., Fischinger, D., Weiss, A., Wolf, D., Vincze, M., Puente, P., Körtner, T., Weninger, M., Papoutsakis, K., Michel, D., et al.: Hobbit: Providing fall detection and prevention for the elderly in the real world. Journal of Robotics **2018** (2018)

[13] Palacín, J., Rubies, E., Clotet, E.: The Assistant Personal Robot Project: From the APR-01 to the APR-02 Mobile Robot Prototypes. Designs **6**(4) (2022) https://doi.org/10.3390/designs6040066

[14] Lynch, K.M., Park, F.C.: Modern Robotics: Mechanics, Planning, and Control, 1st edn. Cambridge University Press, USA (2017)

[15] Maulana, E., Muslim, M.A., Hendrayawan, V.: Inverse kinematic implementation of four-wheels mecanum drive mobile robot using stepper motors. 2015 International Seminar on Intelligent Technology and Its Applications, ISITIA 2015 - Proceeding (May), 51–55 (2015) https://doi.org/10.1109/ISITIA.2015.7219952

[16] Manso, L., Bachiller, P., Bustos, P., Núñez, P., Cintas, R., Calderita, L.: Robocomp: A tool-based robotics framework, vol. 6472 LNAI (2010). https://doi.org/10.1007/978-3-642-17319-6_25